Res Chem Intermed
DOI 10.1007/s11164-013-1429-0

Synthesis and optical properties of 4-(2-{[6-(1,1-dicyanoprop-1-en-2-yl)naphthalen-2-yl] (methyl)amino} ethoxy)-4-oxobutanoic acid fluorescent probe for β-amyloid

HuanBao Fa · JingTing Zhou · Dong Zhang · Wei Yin · HaiFeng Zhang · DanQun Huo · ChangJun Hou · XiaoGang Luo · YaLi Mao · Jin Zhang

Received: 24 March 2013 / Accepted: 30 September 2013

Abstract A novel 4-(2-{[6-(1,1-dicyanoprop-1-en-2-yl)naphthalen-2-yl](methyl) amino} ethoxy)-4-oxobutanoic acid (**5**) fluorescent probe for β-amyloids was synthesized by catalytic acylation using 4-dimethylaminopyridine between succinic anhydride and (1-{6-[(2-hydroxyethyl)(methyl) amino]-2-naphthyl}ethylidene)malononitrile (**4**). The structures of all compounds were identified by proton nuclear magnetic resonance spectroscopy, infrared spectroscopy, mass spectrometry, and ultraviolet–visible (UV–Vis) spectroscopy. The UV–Vis and fluorescence spectra of 1-{6-[(2-hydroxyethyl)(methyl) amino]-2-naphthyl}ethan-1-one (**3**), **4**, and **5** in solvents with different polarities were investigated, and the effects of solvent polarity on the optical properties of the three compounds were studied. The objective product **5** showed high binding affinities toward Aβ(1–40) aggregates in vitro ($K_d = 29.4$ nmol/L) by fluorophotometry. This study provides a powerful fluorescent probe for the molecular diagnosis of Alzheimer's disease.

H. Fa · J. Zhou · W. Yin · H. Zhang · Y. Mao · J. Zhang
College of Chemistry and Chemical Engineering, Chongqing University, Chongqing 400030, China
e-mail: haifengzhang@cqu.edu.cn

H. Fa · D. Huo · C. Hou · X. Luo
Key Laboratory of Biorheological Science and Technology, Ministry of Education, Bioengineering College, Chongqing University, Chongqing 400030, China

H. Fa (✉)
College of Chemistry and Chemical Engineering, Chongqing University, Chongqing 400044, China
e-mail: huanbaofa@cqu.edu.cn

J. Zhou
Third Military Medical University, Chongqing 400038, China

D. Zhang
Department of Radiology, Third Military Medical University, Chongqing 400037, China

Published online: 17 October 2013

Keywords Fluorescent probe · Synthesis · Optical property · β-Amyloid · Alzheimer's disease

Introduction

Alzheimer's disease (AD) is the most common form of dementia affecting millions of people around the world. The clinical symptoms of AD include cognitive decline, irreversible memory loss, disorientation, language impairment, and so on. Major neuropathology observations of postmortem AD brain show the presence of senile plaques (SPs), neurofibrillary tangles (NFTs), and neurophil threads containing β-amyloid aggregates and highly phosphorylated tau proteins. With the aging population, AD is becoming one of the serious problems for human health and living quality [1–3]. Pathogenesis studies showed that SPs and NFTs are hallmark pathologies accompanying neurodegeneration. Furthermore, the growth of β-amyloid plaques in the brain is a major cause of AD [4–7].

In recent years, with the development of medical technology, molecular imaging technologies, such as positron emission tomography (PET), single-photon emission computed tomography, and magnetic resonance imaging (MRI), have been widely used for the early diagnosis of AD. Thus, the design of molecular imaging probes for β-amyloid plaques in the brain has drawn increasing research attention [8, 9]. Several specific binding agents for Aβ are derivatives of naphthalene, benzothiazole, stilbene, or other related heterocyclic derivatives with an electron-donating group on the aromatic rings [10]. However, several studies suggested that analogs of pathological staining dye, such as Chrysamine G and Congo Red [11–13], and styrylbenzenes, such as 1,4-bis(3-carboxy-4-hydroxyphenylethenyl)-benzene (X-34) [14, 15], (*E*,*E*)1-bromo-2,5-bis- (3-hydroxyl carbonyl-4-hydroxy)styrylbenzene (ISB) [16], (*trans*)-1-bromo-2,5-bis-(3-hydroxycarbonyl-4-hydroxy)styrylbenzene (BSB) [17], and (*E*,*E*)-1-iodo-2,5-bis(3-hydroxycarbonyl-4-methoxy)styryl-benzene (IMSB) [18], are not suitable as imaging agents because of their low uptake in the brain. To achieve high brain penetration, the use of neutral, small, and lipophilic compounds is normally considered. 1,1-Dicyano-2-[6-(dimethylamino) naphthalene-2-yl] propene (DDNP), a highly hydrophobic, viscosity-, and solvent-sensitive fluorescent probe has been used previously to label SPs in the brains of AD patients by PET [19, 20, 31].

Considering that the as-synthetic DDNP described by Jacobson et al. [21] had no active group such as carboxyl to bind onto the surface of superparamagnetic iron oxide nanoparticles (SPIONs), a novel MRI contrast agent of SPIONs coated with DDNP for β-amyloid protein was needed. We synthesized a 4-(2-{[6-(1,1-dicyanoprop-1-en-2-yl)naphthalen-2-yl] (methyl)amino} ethoxy)-4-oxobutanoic acid (**5**) fluorescent probe with a –COOH group to target β-amyloid proteins and combine with SPIONs through ligand exchange with oleic acid. Compound **5** was synthesized by treating (1-{6-[(2-hydroxyethyl) (methyl) amino]-2-naphthyl}ethylidene)malononitrile (**4**) with succinic anhydride through catalytic acylation using 4-dimethylamiopryidine (DMAP). Compound **4** was prepared from 2-acetyl-6-methoxy-naphthalene (**1**) by hydrolysis, Bucherer nucleophilic substitution, and Knoevenagel condensation

reactions. The structures of all compounds were identified by proton nuclear magnetic resonance spectroscopy (^{1}H NMR), infrared spectroscopy (IR), magnetic spectrometry (MS), and ultraviolet–visible (UV–Vis) spectroscopy. The UV–Vis and fluorescence spectra of 1-{6-[(2-hydroxyethyl)(methyl)amino]-2-naphthyl}ethan-1-1 (**3**), **4**, and **5** in solvents of different polarities were investigated, and the effects of solvent polarity on the optical properties of the three compounds were studied. The objective product 5 showed high binding affinities toward Aβ(1–40) aggregates in vitro (K_d = 29.4 nmol/L) by fluorophotometry. This study provides a powerful fluorescent probe for the molecular diagnosis of AD. The synthetic route of compound **5** is shown in Scheme 1.

Experimental

Apparatus

^{1}H NMR spectra were obtained using a Brucker 500MHZ spectrometer. IR spectra were obtained using a Nicolet Shimadzu Fourier transform-infrared

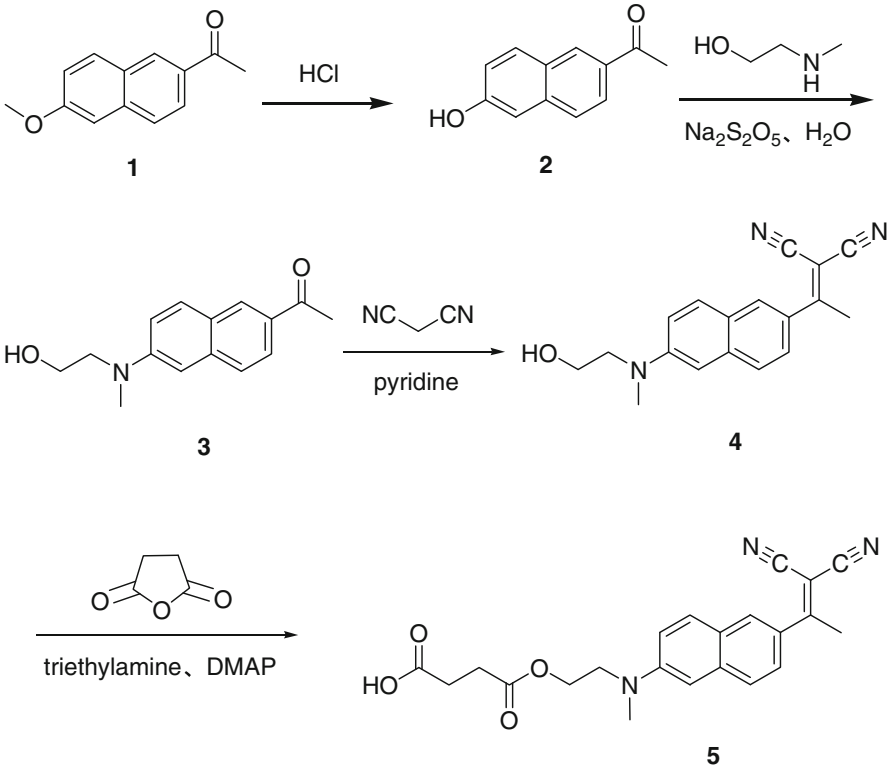

Scheme 1 Synthetic routes of compound **5**

spectrophotometer. UV–Vis spectra were recorded on an Analytik Jena SPECORD 200 spectrophotometer. Fluorescence spectra were determined using a Shimadzu RF-5301 spectrophotometer. MS spectra were obtained with a VG Auto Spec-3000 spectrophotometer. The melting points were measured using an SGW X-4 microscopic melting point apparatus.

Materials

DMAP, succinic anhydride, triethylamine, EtOH, and ethyl acetate were purchased from Aladdin, Shanghai, China. Compound **1** was obtained from Tokyo Chemical Industry, Japan. The in vitro binding experiment was carried out at 37 °C in a pH 7.4 phosphate-buffered medium. Sodium dihydrogen phosphate and disodium hydrogen phosphate were purchased from Xiya, Chengdu. β-amyloid was obtained from Merck, Taiwan. All other chemicals were of analytical grade.

Synthesis of compound **5**

*1-(6-Hydroxy-2-naphthyl)-1-ethanone (**2**)*

Compound **2** was prepared in accordance to a previous method [22]. A solution of 350 mL of HCl ($d = 1.16$) was stirred in a three-neck round-bottom flask and heated to boiling. Subsequently, a solution of 1.212 g (6.06 mmol) of 1-(6-methoxy-2-naphthyl)-1-ethanone (**1**) in a minimum amount of dichloromethane was added, and the mixture was stirred and heated at reflux for 2 h. The hot solution was filtered through a mineral wool plug to remove the oily residue. The solid that separated after cooling was filtered through a glass frit and dissolved in 26 mL of ethyl acetate. The solution was washed with brine, dried over anhydrous magnesium sulfate, and evaporated to yield a product of 1 g (84 %). After recrystallization from triethylamine, the sample was melted at 174–177 °C (Ref. [22]: 173.5–177 °C); UV–Vis (EtOH) λ_{max} 317 nm; ^{1}H NMR (DMSO-d_6, 500 MHZ) δ 2.650 (s, 3H, $COCH_3$), 7.173 (d, $J = 8.5$ Hz, 1H, H–C^7), 7.193 (d, 2.5 Hz, 1H, H–C^5), 7.750 (d, $J = 9$ Hz, 1H, H–C^4), 7.864 (dd, $J = 8.5$ and 2.5 Hz, 1H, H–C^8), 7.971 (d, $J = 9$ Hz, 1H, H–C^3), 8.537 (s, 1H, H–C^1), 10.212 (s, 1H, OH); IR (KBr) ν/cm^{-1} 3,362.0, 3,073.7, 2,999.7, 2,926.0, 1,661.7, 1,627.5, 1,582.9, 1,570.4, and 1,207.1.

*Compound **3***

Compound **3** was prepared by Bucherer nucleophilic substitution reaction as described previously [23]. Briefly, a mixture of compound 2 (744 mg, 3.92 mmol), sodium metabisulfite (3.5 g, 18 mmol), 2-ethylaminoethanol (5.2 mL, 64 mmol), and water (34 mL) was heated in an autoclave at 125–130 °C for 64 h. After cooling, the mixture was evaporated to dryness. The residue was treated with CH_2Cl_2/CH_3OH (8:2) and filtered. The filtrate was evaporated and purified by chromatography on silica gel and eluted stepwise with CH_2Cl_2, CH_2Cl_2/EtOAc (98:2), and CH_2Cl_2/EtOAc (96:4) to yield a product of 671 mg (Yield, 67.2 %). M.p. 99.5–105 °C (Ref. [23]: 105.5–106 °C); thin-layer chromatography (TLC): R_f

0.4 (CH_2Cl_2/EtOAc V:V = 98:2); TLC: R_f 0.4 (CH_2Cl_2/EtOAc V:V = 98:2); UV–Vis (EtOH) λ_{max} 373 nm; ^{1}H NMR (DMSO-d_6, 500 MHZ) δ 2.602 (s, 3H, CH_3), 3.071 (s, 3H, NCH_3), 3.573 (t, J = 6 Hz, 2H, NCH_2), 3.828 (t, J = 6 Hz, 2H, OCH_2), 7.115 (d, J = 2.3 Hz, 1H, H–C^5), 7.178 (dd, J = 8.6 and 2.3 Hz, 1H, H–C^7), 7.556 (d, J = 8.2 Hz, 1H, H–C^4), 7.719 (d, J = 8.6 Hz, 1H, H–C^8), 7.846 (d, J = 8.2 HZ, 1H, H–C^3), 8.243 (s, 1H, H–C^1); IR (KBr) ν/cm^{-1} 3,458.9, 3,063.6, 2,933.8, 2,881.3, 1,669.0, 1,651.0, 1,621.2, 1,508.2, 1,490.7, and 1,204.7.

Compound ***4***

A solution of compound 3 (421 mg, 1.73 mmol) and malononitrile (4.5 mL, 6.93 mmol) in pyridine (10 mL) was stirred and heated at 105–110 °C under a slow stream of argon for 24 h. TLC indicated full consumption of the starting material. The reaction mixture was evaporated and then coevaporated at least twice with toluene to remove pyridine. The crude reaction mixture was purified by column chromatography on silica gel and eluted stepwise with CH_2Cl_2, CH_2Cl_2/EtOAc (98:2), and CH_2Cl_2/EtOAc (95:5) to give a product of 411 mg, (Yield, 82.6 %). TLC: R_f 0.42 (CH_2Cl_2/EtOAc 95:5); M.p. 126–129.5 °C (Ref. [23]: 128–131 °C); UV–Vis (EtOH) λ_{max} 438 nm; ^{1}H NMR (DMSO-d_6, 500 MHZ) δ 2.688 (s, 3H, CH_3), 3.091 (s, 3H, NCH_3), 3.571 (t, J = 4.5 Hz, 2H, NCH_2), 3.610 (t, J = 4.5 Hz, 2H, OCH_2), 4.752 (t, J = 4.5 Hz, 1H, OH), 6.955 (s, 1H, H–C^5), 7.295 (d, J = 9 Hz, 1H, H–C^7), 7.626 (d, J = 8.5 Hz, 1H, H–C^3), 7.704 (d, J = 8.5 Hz, 1H, H–C^4), 7.817 (d, J = 9 Hz, 1H, H–C^8), 8.168 (s, 1H, H–C^1); IR (KBr) ν/cm^{-1} 3,512.4, 3,074.8, 2,923.4, 2,223.8, 1,620.5, 1,546.2, 1,504.4, and 1,188.9.

Compound ***5***

A mixture of succinic anhydride (125 mg, 1.25 mmol), DMAP (124 mg, 1 mmol), and water-free CH_2Cl_2 (10 mL) was magnetically stirred at room temperature under nitrogen for 30 min. Subsequently, 291 mg (1 mmol) of compound **4** and 140 μL of water-free triethylamine were added. The reaction mixture was continuously stirred overnight at room temperature. The solution was then evaporated to dryness. The residue was purified by chromatography on silica gel and eluted stepwise with CH_2Cl_2, CH_2Cl_2/CH_3OH (99:1), and CH_2Cl_2/CH_3OH (98:2) to give a product of 211 mg (Yield, 54.1 %). M.p. 135.8–137.2 °C; UV–Vis (CH_2Cl_2) λ_{max} 432 nm; ^{1}H NMR (DMSO-d_6, 500 MHZ) δ 2.425 (s, 4H, CO–CH_2–CH_2–CO), 2.699 (s, 3H, C=CCH_3), 3.090 (s, 3H, N–CH_3), 3.773 (t, J = 5.5 Hz, 2H, N–CH_2), 4.244 (t, J = 5.5 Hz, 2H, O–CH_2), 7.013 (s, 1H, H–C^5, 7.322 (dd, J = 2.5 and 9 Hz, 1H, H–C^4), 7.644 (dd, J = 2.5 and 9 Hz, 1H, H–C^8), 7.738 (d, J = 9 Hz, 1H, H–C^7), 7.850 (d, J = 9 Hz, 1H, H–C^3), 8.190 (s, 1H, H–C^1), 12.234 (s, 1H, COOH); IR (KBr) ν/cm^{-1} 3,438.4, 3,013.1, 2,959.8, 2,924.9, 2,215.6, 1,728.1, 1,705.5, 1,618.1, 1,532.9, 1,505.3, and 1,167.7; MS (70 eV) m/z %: 390.1 (M^+).

Solution preparation

Spectral analysis

Compounds **1**–**5** were dissolved in EtOH to obtain a final concentration of 2×10^{-5} mol dm^{-3} and then the UV–Vis and fluorescence spectra were studied.

Solvent effects

Compounds **3**, **4**, and **5** were dissolved in nine solvents including cyclohexane, toluene, CH_2Cl_2, $CHCl_3$, $CH_3COOC_2H_5$, EtOH, CH_3OH, PBS, (pH 7.4), and AcOH to obtain a final concentration of 2×10^{-5} mol dm^{-3}. In the phosphate buffer solution (PBS) and cyclohexane solutions, compounds **3**, **4**, and **5** were initially dissolved in a minimum amount of methanol and diluted by PBS and cyclohexane to obtain the desired concentration. The spectral shift will be less than 0.5 nm and could be negligible when the methanol concentration is less than 2 % [24]. The UV–Vis and fluorescence spectra of the above solutions were determined.

Binding of compound **5** to Aβ(1–40) fibril in vitro

Aβ(1–40) fibril formation

Aβ(1–40) fibrils were prepared as described previously [25]. Briefly, 0.5 mg of Aβ(1–40) was dissolved in 1 mL of PBS (pH 7.4) and mixed with a magnetic stir bar for 3 days at 37 °C in a bed temperature incubator. The solution became visibly cloudy. The fibrils were used immediately after their production was confirmed.

*Binding of compound **5** to Aβ(1–40) fibril*

Fresh solutions of compound **5** in EtOH were appropriately diluted with PBS (pH 7.4) to obtain the following series of concentrations: 0.1, 0.5, 1.0, 1.5, 2.0, 2.5, 3.0, 3.5, and 4.0×10^{-7} mol/L. Each solution was treated as follows: first, 300 μL of compound **5** was pipetted into a 500-μL cuvette; second, 5 μL of Aβ solution and 300 μL of compound **5** solution were pipetted into another 500-μL cuvette; finally, the two solutions were placed in a bed temperature incubator at 37 °C and 300 r/min for 15 min. The fluorescence intensity of each sample was measured (integrated peak area) three times with three parallels at $\lambda_{ex} = 440$ nm using a fluorescence spectrophotometer. The binding of compound **5** to Aβ(1–40) was illustrated by a double-reciprocal plot, with the compound **5** concentration as the abscissa and the reciprocal of fluorescence intensity difference between the two solutions as the vertical axis.

Results and discussion

Recrystallization of compound **2**

Previous studies indicated that the recrystallization solvent of compound **2** is ethyl acetate [22]. In our study, triethylamine was used as the recrystallization solvent for compound **2**, which is weakly acidic and easily soluble in alkaline triethylamine, and the neutral impurities are insoluble in triethylamine. Compound **2** was easily separated by a suction filter, and the filtrate was neutralized with diluted HCl. The white crystal 2 could be obtained from the filtrate. The purification result was better than that reported previously [22].

IR spectra

The IR spectra of compounds **4** and **5** in Fig. 1 show a broad absorption band at 3,550 cm^{-1}(ν_{O-H}) to 3,390 cm^{-1}(ν_{O-H}), which implied the presence of a hydroxyl group in the compound. The broad peak from 2,850 to 2,930 cm^{-1} represented the stretching vibration of C–H, and the peak from 2,230 to 2,210 cm^{-1} was assigned to the stretching vibration of C≡N. The peaks at 1,504, 1,533, and 1,618 cm^{-1} were characteristic absorption peaks of the aromatic rings. The C–O stretching vibration at 1,188.9 and 866 cm^{-1} was assigned to the bending vibration of C–H in the aromatic ring plane. Compared with compound **4**, compound **5** had an anhydride group, which indicated that their IR spectra were basically the same. The characteristic absorption bands of the anhydride group at 1,728.1 cm^{-1} ($\nu_{C=O}$ in carboxyl group) and 1,705.5 cm^{-1}($\nu_{C=O}$ in ester group) were found in the IR spectra of compound **5**. The bands at 1,100–1,120 cm^{-1} were attributed to the bending vibration of C–O and C–N.

^{1}H NMR of compound 5

The chemical structure of compound **5** was characterized by ^{1}H NMR in deuterated dimethyl sulfoxide (DMSO-d_6) solution, and the results are shown in Fig. 2. The hydrogen atoms of compound **5** were marked as 1, 2, 3, 4, 5, 6, and 7. As shown in the figure, the signals at 2.425 and 12.234 ppm were attributed to the signals of 1 proton of –$COCH_2CH_2CO$– and 7 protons of –COOH, respectively. The singlet peaks at 2.699 and 3.090 ppm were ascribed to =CCH_3 and –NCH_3, respectively. The three sharp peaks at 3.763–3.784 and 4.246–4.266 ppm were attributed to the methylene protons of –NCH_2 and –OCH_2, respectively. The peaks of the 6 protons of the aromatic ring were found at 7.013–8.190 ppm.

UV–Vis spectra

Figure 3 shows the UV–Vis spectra of compounds **1**–**5** in EtOH solution. The absorption bands at 210–250, 255–270, and 270–550 nm were attributed to the E_1, E_2, and B characteristic bands of the naphthalene ring, respectively. The B band

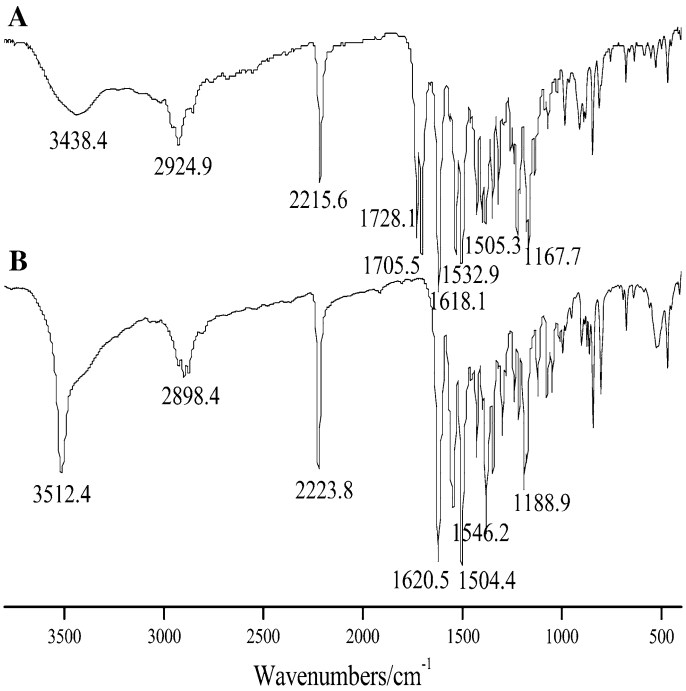

Fig. 1 IR spectra of compound **5** (*a*) and compound **4** (*b*)

originally possessed a vibrational and rotational fine structure. However, considering that the naphthalene derivatives were affected by polar solvent molecules and could not rotate freely, the fine structure of the B absorption band of the five compounds disappeared completely and became a broad absorption band [26]. In addition, the 6-position of the naphthalene ring was replaced by the auxochromic group –OR, –OH, or $–NR_2$ whose lone electron pairs could form p-π conjugated systems. The conjugation effect led to the red shift of the B absorption band.

As shown in Fig. 3, the maximum absorption wavelengths of the B absorption band of the five compounds were 308, 317, 373, 438, and 432 nm. The 6-position of the naphthalene ring of compound **3** was replaced by $–NR_2$. 2-Hydroxyethyl methylamino is a strong electron donor group and can increase the electron cloud density of the naphthalene ring. Thus, compared with compound **2**, the B absorption band of compound **3** showed a red shift of 56 nm. However, the B absorption band of compound **4** showed a red shift of 65 nm compared with compound **3** after introduction of the chromophore $–C=C(CN)_2$ to the 2-position of the naphthalene ring by Knoevenagel condensation reaction between compound **3** and malononitrile, which enhanced the conjugated system of compound **4**. Ester and carboxyl groups were introduced to compound **5** by acylation between succinic anhydride and compound **4**. Compared with compound **4**, compound **5** showed a blue shift of 6 nm in the B absorption band. The electron-withdrawing C=O groups reduced the conjugation effect of $–NR_2$ when naphthalene was reduced.

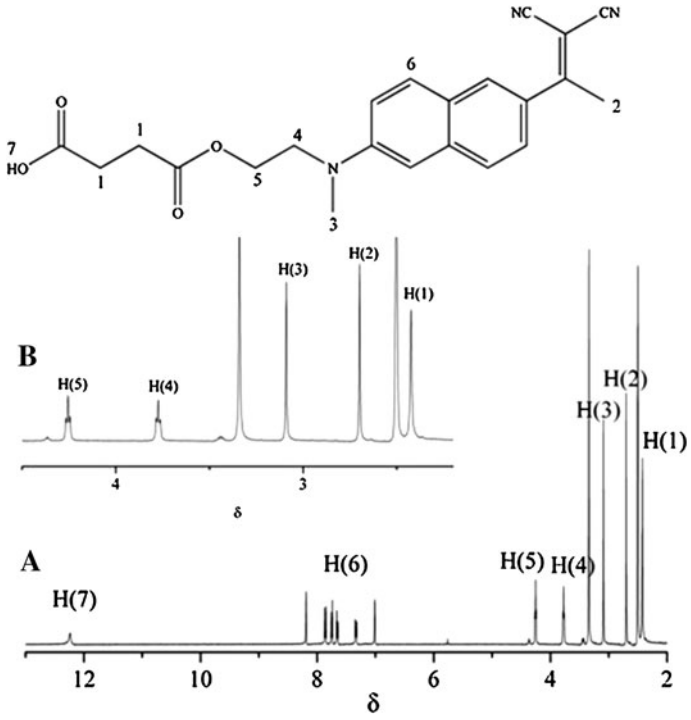

Fig. 2 ^{1}H NMR of compound **5**

Different solvents have different impacts on the absorption wavelength and intensity of the UV–Vis spectra [27]. To investigate the behavior of compounds **3**, **4**, and **5** in different solutions, their UV–Vis spectra were measured in nine solvents of various polarities, including cyclohexane, toluene, ethyl acetate, methylene chloride, chloroform, acetic acid, EtOH, methanol, and PBS. The maximum absorption wavelength (λ_{max}) and molar extinction coefficient of the three compounds are shown in Table 1. The results indicated that the UV–Vis spectra of the three compounds were highly dependent on the nature of the solvent. A stronger solvent polarity resulted in a greater red-shift degree of the maximum absorption wavelength. With enhanced solvent polarity, the decrease in the π* molecular orbital energies of compounds **3**, **4**, and **5** was larger than the ground state π orbital energy. Thus the $\pi \rightarrow \pi^*$ transition energy change ΔE was reduced and λ_{max} was red-shifted [27]. As shown in Table 1, the λ_{max} range of compounds **3**, **4**, and **5** in the nine solvents were 343–381, 423–441, and 421–437 nm, respectively. The molar extinction coefficient data indicated that compounds **3** and **4** possessed maximum absorbance in methanol and minimum absorbance in dichloromethane, whereas compound **5** possessed maximum absorbance in EtOH and minimum absorbance in PBS and acetic acid.

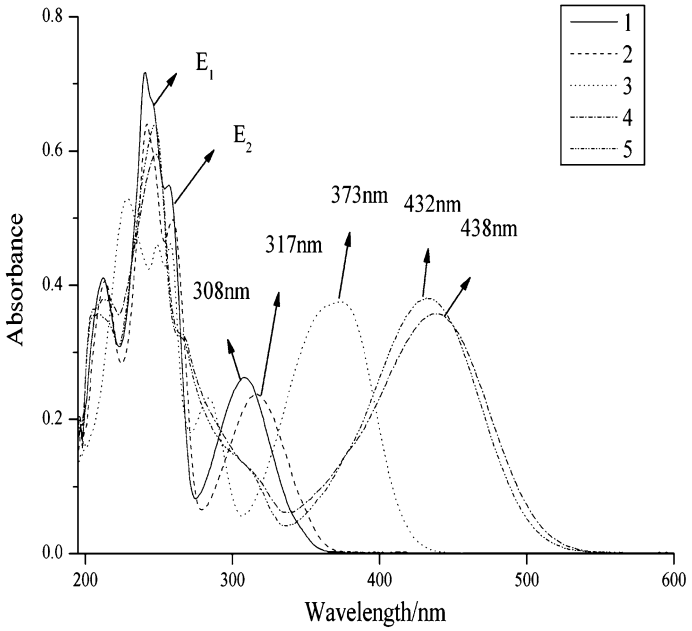

Fig. 3 UV–Vis spectra of compounds **1–5**, final concentration in ethanol 5×10^{-6} mol/L

Table 1 λ_{max} and ε for compounds **3–5** in different solvents

Solvent	PBS	MeOH	EtOH	AcOH	$CHCl_3$	CH_2Cl_2	$CH_3COOC_2H_5$	$PhCH_3$	CyH
$E_T(30)^{25}$	63.1	55.4	51.9	51.7	41.1	39.1	38.1	33.9	30.9
λ_{max} (nm)									
3	381	374	373	376	357	354	352	350	343
4	441	439	438	433	437	435	432	432	423
5	437	434	432	428	431	431	426	422	421
$\varepsilon(1 \times 10^{-4})$ (dm^3 mol^{-1} cm^{-1})									
3	1.7	2.2	1.8	1.8	1.8	1.6	2.0	1.8	1.7
4	1.8	1.9	1.7	1.8	1.7	1.6	1.7	1.7	1.8
5	1.7	1.8	1.9	1.7	1.8	1.8	1.8	1.8	1.8

PBS phosphate-buffered saline (pH 7.4), $E_T(30)^{25}$ empirical parameters of solvent polarity, the higher value of $E_T(30)^{25}$, the greater solvent polarity

Fluorescence spectrum

Compound **5** was developed as a lipophilic probe for fluorescence spectroscopy to target β-amyloid [28]. Figures 4 and 5 show excitation spectra and emission spectra of compounds **1–5** in 10^{-6} mol/L EtOH. From Fig. 4, the excitation maxima of compounds **1–5** were 324, 334, 379, 458, and 462 nm respectively. Considering the highly conjugated aromatic systems and rigid plane structures of compounds **1–5**,

their lowest singlet excited states (S_1) were $\pi \rightarrow \pi^*$ transition, and they all had excellent fluorescence performance [21]. The emission maxima of compounds **1**–**5** were observed at 421, 427, 483, 575, and 566 nm, respectively. The hydroxyl group at the 6-position of compound **2** was substituted by $-NR_2$. $-NR_2$ is an electron-donating group and its electron cloud is parallel to the π orbits of the aromatic ring to form p–π conjugation, which resulted in the approximately 56-nm red shift of the maximum emission peak and the increase in the fluorescence intensity of compound **3**. The introduction of the chromophore $-C{=}C(CN)_2$ group increased the conjugate system and conjugate degree of compound **4**. Thus, the non-localized π electrons were easily excited, and the fluorescence spectrum changed obviously with a 92-nm red shift. Compared with compound **4**, the maximum emission peak of compound **5** was blue-shifted by 9 nm, and the fluorescence intensity was decreased. These spectral changes were attributed to the ester and carboxyl groups of compound **5**. The C=O in compound **5** is an electron-withdrawing group that reduced the electron density of $-NR_2$, which weakened the conjugate interaction between $-NR_2$ and the aromatic ring.

The physical constants (dipole moment, dielectric constant, and refractive index) of the nine solvents and the fluorescence excitation wavelength (λ_{ex}), emission wavelength (λ_{em}), and Stokes shift of compounds **3**, **4**, and **5** in the nine different-polarity solvents are shown in Table 2. The results indicated that the λ_{ex} and λ_{em} of compounds **3**, **4**, and **5** showed a significant red shift when the solvent polarity was enhanced. The fluorescence maximum emission ranges of the three compounds were 395–492, 474–585, and 465–575 nm. Compound **5** possessed maximum λ_{em} in

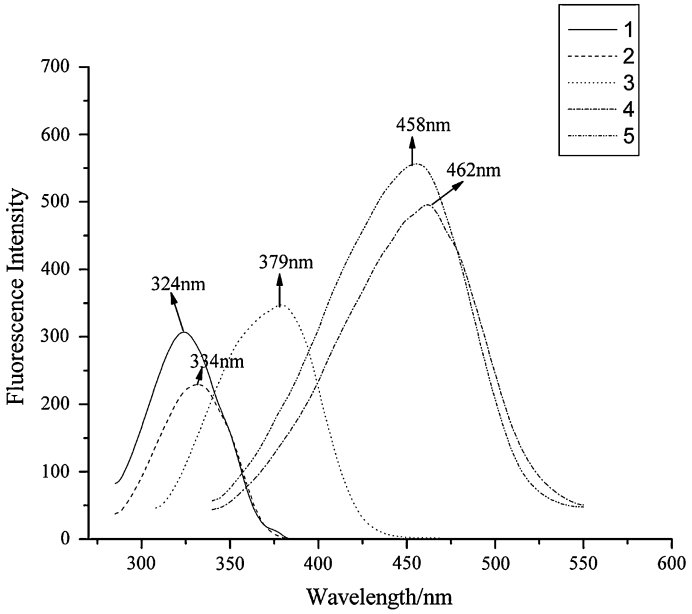

Fig. 4 The excitation spectra of compounds **1**–**5**, final concentration in ethanol 5×10^{-6} mol/L

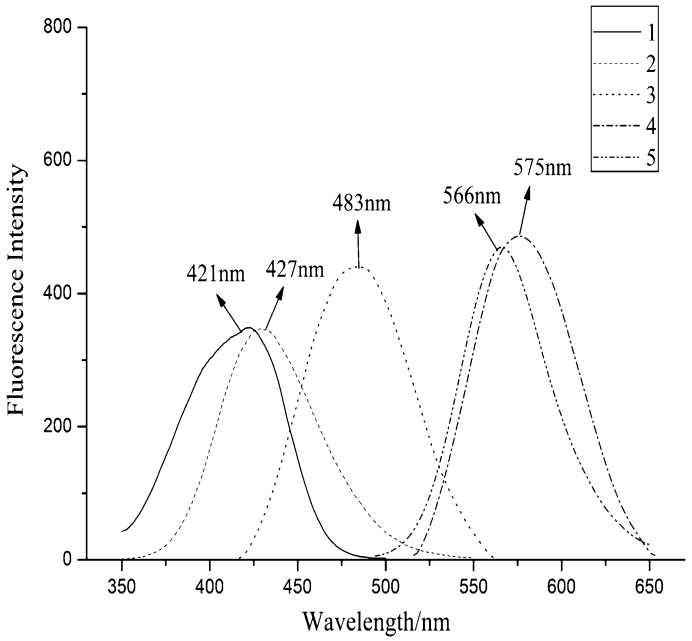

Fig. 5 The emission spectra of compounds **1**–**5**, final concentration in ethanol 5×10^{-6} mol/L

EtOH and minimum λ_{em} in cyclohexane. The solvent effect indicated that compounds **3**, **4**, and **5** were intramolecular electron-transfer complexes, the electrons of which transfer from the electron donor $-NR_2$ to the electron acceptor naphthalene ring. Compounds **3**, **4**, and **5** were neutral molecules in the ground state, but their polarities were increased when their π electrons were excited. The stabilization role of solvents in the excited states was stronger than in the ground state in the polar solvent. Thus, the transition energy was reduced with the increase in solvent polarity, and the maximum emission peak was red-shifted [28].

The dipole moment change in compound **5** at ground state and excited state could be calculated by the Lippert equation:

$$\upsilon_a - \upsilon_f \cong \frac{2}{hc}\left(\frac{\varepsilon - 1}{2\varepsilon + 1} - \frac{n^2 - 1}{2n^2 + 1}\right)\frac{(\mu^* - \mu)^2}{a^3} + k, \quad (1)$$

where v_α and v_f are the absorption and emission wave numbers in the same solvent, respectively, $(v_\alpha - v_f)$ is the Stokes shift, h is the Planck constant, c is the speed of light, ε and n are the dielectric constant and refractive index of the solvent, respectively, μ^* and μ are the electronic dipole moment of the compound at excited state and ground state, respectively, and a is the ball volume radius of the solute molecules in solution. According to the crystallography data of naphthalene derivatives, the distance from N to O of compound **5** is approximately 0.84 nm [29]. In Eq. 1, the directional polarization rate Δf is as follows:

Table 2 Fluorescence property of compounds **3–5** in different solvents

Solvent	PBS	MeOH	EtOH	AcOH	$CHCl_3$	CH_2Cl_2	$CH_3COOC_2H_5$	$PhCH_3$	CyH
Dipole moment (μ/D)	1.85	1.70	1.69	1.74	1.15	1.60	1.78	1.23	0.00
Dielectric constant (ε)	78.5	33.6	24.30	6.15	4.81	8.90	6.03	2.37	1.18
Refractive index (n^{D25})	1.3330	1.3290	1.3618	1.3716	1.4467	1.4244	1.3720	1.4961	1.4626
Oriented polarizability	0.320	0.308	0.298	0.203	0.185	0.209	0.199	0.013	0.001
$E_T(30)^{25}$	63.1	55.4	51.9	51.7	41.1	39.1	38.1	33.9	30.9
λ_{ex} (nm)									
3	376	380	379	368	371	369	356	352	348
4	443	448	443	441	439	436	437	427	420
5	440	443	439	439	431	429	433	425	418
λ_{em} (nm)									
3	492	492	483	466	450	443	451	421	395
4	583	585	575	561	535	522	515	489	474
5	571	575	566	554	528	520	511	476	465
Stokes shift (cm^{-1})									
3	6,270.5	5,990.6	5,681.3	5,716.7	4,731.9	4,526.9	5,149.5	4,024.9	3,419.2
4	5,420.7	5,227.4	5,182.1	4,850.4	4,087.5	3,778.7	3,465.8	2,969.3	2,712.5
5	5,214.1	5,182.1	5,111.2	4,728.5	4,262.5	4,189.2	3,525.2	2,521.0	2,418.1

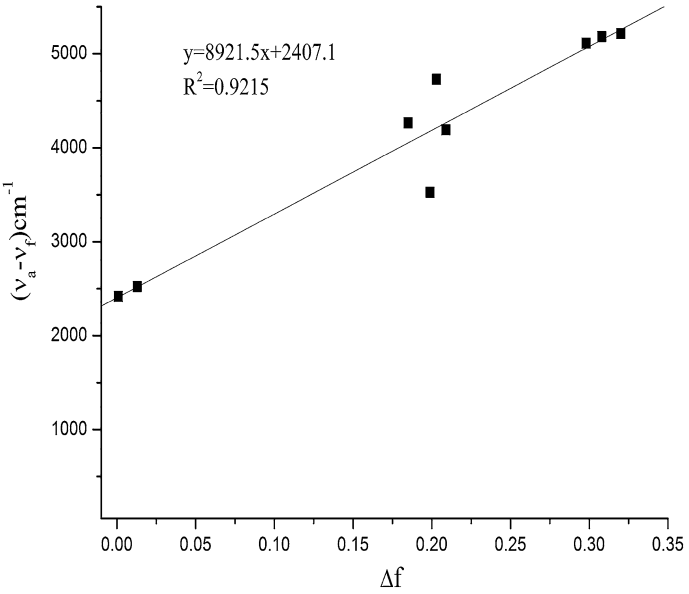

Fig. 6 Stokes shift of compound **5** versus Δf values

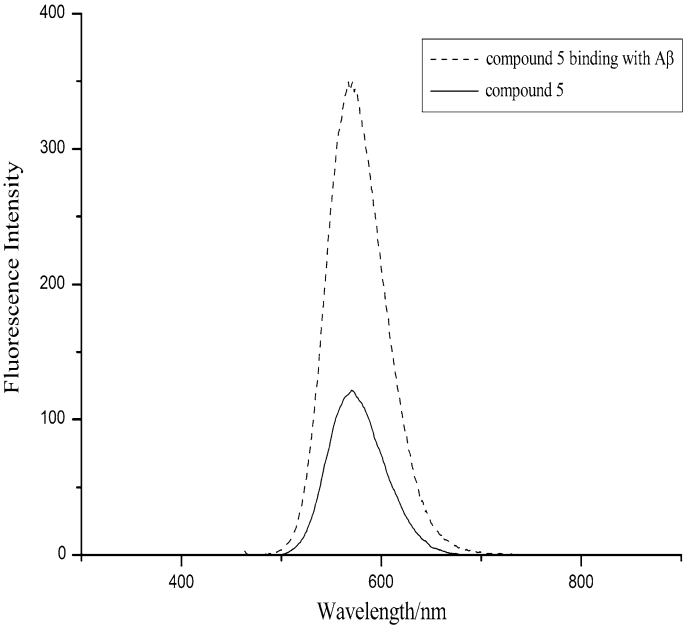

Fig. 7 Fluorescence enhancement of compound **5** binding with Aβ(1–40), final concentration 4×10^{-7} mol/L in PBS

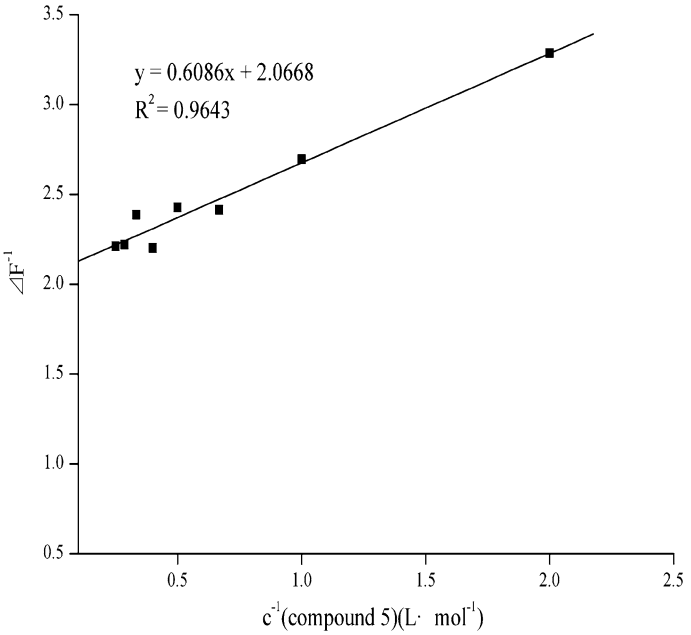

Fig. 8 Double reciprocal illustration of compound **5** band with Aβ(1–40)

$$\Delta f = \frac{\varepsilon - 1}{2\varepsilon + 1} - \frac{n^2 - 1}{2n^2 + 1}. \tag{2}$$

As shown in Fig. 6, the straight line represents the mapping of the Stokes shifts of compound **5** in different solvents with Δf. The slope of the line was 8,921.5, $R^2 = 0.9215$. The dipole moment change of compound **5** at ground state and excited state was 7.25 D, which was calculated using the line slope and the Lippert equation. The intramolecular electron transfer in compound **5** was induced after excitation, which resulted in intramolecular electron rearrangement. Such rearrangement increased the dipole moment difference between the excited state and the ground state. Electronic rearrangement in the solvent molecules around compound **5** was likewise induced to adapt to the new charge distribution of compound **5**. This result narrowed the energy gap between the excited state and the ground state. Thus, the increase in solvent polarity caused the red shift in the maximum emission peak.

Binding of compound **5** to Aβ(1–40) fibrils in vitro

Figure 7 shows the fluorescence spectrum of compound **5** with 4×10^{-7} mol/L in PBS binding to Aβ(1–40). An enhanced fluorescence emission was observed upon binding of the Aβ(1–40) fibrils to compound **5**. The strong viscosity of Aβ(1–40) fibrils limited the intramolecular rotational relaxation of compound **5** and induced compound **5** to form a rigid plane structure that could improve the fluorescence quantum yield and enhance the fluorescence integral intensity of compound **5** [30].

The double reciprocal illustration of compound **5** binding to Aβ(1–40) was used to study the combination of K_d in Fig. 8, with the concentration of compound **5** as the abscissa and the reciprocal of fluorescence intensity difference between the two solutions as the vertical axis. As shown in Fig. 8, the intersection between the straight lines and the *x*-axis was $-1/K_d = -3.39$ and $K_d = 29.4$ nmol/L. K_d was inversely proportional to the affinity of the molecules. The results showed that compound **5** has potential for the early detection and monitoring of the progression of AD.

Conclusions

We designed and synthesized a 4-(2-{[6-(1,1-dicyanoprop-1-en-2-yl) naphthalen-2-yl](methyl)amino}ethoxy)-4-oxobutanoic acid fluorescent probe for β-amyloid that can be used for the early detection of AD. The structures of all compounds were confirmed by ^{1}H NMR, IR, MS, and UV–Vis techniques. The UV–Vis and fluorescence spectra of compounds **3**, **4**, and **5** in the nine solvents with various polarities were investigated, and the effects of solvent polarity on the optical properties of the three compounds were studied. The solvent effect indicated that λ_{max}, λ_{ex}, and λ_{em} were red-shifted with the increase in solvent polarity. According to the Lippert equation, the dipole moment change of compound **5** between the ground state and excited state was 7.25 D. This result caused the electrons of the solvent molecules around compound **5** to undergo electronic rearrangement. Such rearrangement narrowed the energy gap between the excited state and ground state and caused the red shift in the maximum emission peak with the increase in solvent polarity. Compound **5** showed high binding affinity toward Aβ(1–40) aggregates in vitro ($K_d = 29.4$ nmol/L) by fluorophotometry. These results suggest that compound **5** can be used for the early detection and monitoring of the progression of AD. The conjugation of compound **5** with SPIONs to obtain an MRI contrast agent shall be further studied.

Acknowledgments We gratefully acknowledge the support of this research by National natural science funds (NSFC, No. 30970799, 31101284), Natural Science Foundation Project of CQ CSTC (No. CSTC, 2008BB5285, 2010BB1209), Central College Operational costs of basic research (No. CQDXWL-2012-034, CQDXWL-2012-035).

References

1. X.J. Chen, Advances in imaging agents for β-amyloid plaques. Prog. Chem. **19**, 122–129 (2007)
2. J. Hardy, D.J. Selkoe, The amyloid hypothesis of Alzheimer's disease: progress and problems on the road to therapeutics. Science **297**, 353–356 (2002)
3. R.N. Rosenberg, Explaining the cause of the amyloid burden in Alzheimer disease. Arch. Neurol. **59**, 1367–1368 (2002)
4. J.C. Vickers, T.C. Dickson, P.A. Adlard, H.L. Saunders, C.E. King, G. McCormack, The cause of neuronal degeneration in Alzheimer's disease. Prog. Neurobiol. **60**, 139–165 (2000)
5. D.P. Salmon, K.L. Lange, Cognitive screening and neuropsychological assessment in early Alzheimer's disease. Clin. Geriatr. Med. **17**, 229–254 (2001)

6. D.J. Selkoe, Cell biology of the amyloid beta-protein precursor and the mechanism of Alzheimer's disease. Annu. Rev. Cell Biol. **10**, 373–403 (1994)
7. D.B. Teplow, Structural and kinetic features of amyloid β-protein fibrillogenesis. Amyloid **5**, 121–142 (1998)
8. A. Kurihara, W.M. Pardridge, In chelation, conjugation to poly (ethylene glycol)-biotin linkers, and autoradiography with Alzheimer's disease brain sections. Bioconjug. Chem. **11**, 380–386 (2000)
9. C.W. Dicus, D. Willenbring, M.H. Nantz, Synthesis of $^{13}C_1$-pinonaldehyde. J. Label. Compd. Radiopharm. **48**, 223–229 (2005)
10. H.F. Kung, Imaging of Aβ plaques in the brain of Alzheimer's disease. Int. Congr. Ser. **1264**, 3–9 (2004)
11. G.W. Kabalka, V. Namboodiri, M.R. Akula, Synthesis of 123I labeled Congo Red via solid-phase organic chemistry. J. Label. Compd. Radiopharm. **44**, 921–929 (2001)
12. W. Zhen, H. Han, M. Anguiano, C.A. Lemere, C.G. Cho, P.T. Lansbury Jr, Synthesis and amyloid binding properties of rhenium complexes: preliminary progress toward a reagent for SPECT imaging of Alzheimer's disease brain. J. Med. Chem. **42**, 2805–2815 (1999)
13. N.A. Dezutter, T.J. de Groot, R.H. Busson, G.A. Janssen, A.M. Verbruggen, Preparation of 99mTc-N2S2 conjugates of chrysamine G, potential probes for the beta-amyloid protein of Alzheimer's disease. J. Label. Compd. Radiopharm. **42**, 309–324 (1999)
14. C.A. Mathis, D.P. Holt, Y. Wang, M.L. Debnath, B.J. Bacskai, B.T. Hyman, W.E. Klunk, In vivo evaluation and imaging of a lipophilic derivative of Congo Red for amyloid assessment. J. Nucl. Med. **42**, 252 (2001). (abstract)
15. S.D. Styren, R.L. Hamilton, G.C. Styren, W.E. Klunk, X-34, a fluorescent derivative of Congo Red: a novel histochemical stain for alzheimer's disease pathology. J. Histochem. Cytochem. **48**, 1223–1232 (2000)
16. C.-W. Lee, Z.-P. Zhuang, M.-P. Kung, K. Plossl, D. Skovronsky, T.L. Gur, C. Hou, J.Q. Trojanowski, V.M.-Y. Lee, H.F. Kung, Isomerization of (*Z*,*Z*) to (*E*,*E*)1-bromo-2,5-bis-(3-hydroxy carbonyl-4-hydroxy)styrylbenzene in strong base: probes for amyloid plaques in the brain. J. Med. Chem. **44**, 2270–2275 (2001)
17. D.M. Skovronsky, D.M. Skovronsky, B. Zhang, M.-P. Kung, H.F. Kung, J.Q. Trojanowski, V.M.-Y. Lee, In vivo detection of amyloid plaques in a mouse model of alzheimer's disease. Proc. Natl. Acad. Sci. USA **97**, 7609–7614 (2000)
18. Z.-P. Zhuang, M.P. Kung, C. Hou, D.M. Skovronsky, T.L. Gur, K. Plössl, J.Q. Trojanowski, V.M.-Y. Lee, H.F. Kung, Radioiodinated styrylbenzenes and thioflavins as probes for amyloid aggregates. J. Med. Chem. **44**, 1905–1914 (2001)
19. E.D. Agdeppa, V. Kepe, A. Petric, N. Satyamurthy, J. Liu, S.-C. Huang, G.W. Small, G.M. Coled, J.R. Barrio, In vitro detection of (*S*)-naproxen and ibuprofen binding to plaques in the Alzheimer's brain using the positron emission tomography molecular imaging probe 2-(1-{6-[(2-[18*F*]fluoroethyl)(methyl)amino]-2-naphthyl}ethylidene)malononitrile. Neuroscience **117**, 723–730 (2003)
20. K. Shoghi-Jadid, G.W. Small, E.D. Agdeppa, V. Kepe, L.M. Ercoli, P. Siddarth, S. Read, N. Satyamurthy, A. Petric, S.C. Huang et al., Localization of neurofibrillary tangles and beta-amyloid plaques in the brains of living patients with alzheimer disease. Am. J. Geriatr. Psychiatry **10**, 24–35 (2002)
21. A. Jacobson, A. Petric, D. Hogenkamp, A. Sinur, R.J. Barrio, 1,1-Dicyano-2-[6-(dimethylamino)-2-naphthalenyl]propane: a solvent polarity and viscosity sensitive fluorophore for fluorescence microscopy. J. Am. Chem. Soc. **118**, 5572–5579 (1996)
22. P. Andrej, S. Tatjana, R.B. Jorge, Novel fluorescent reactive dyes as intermediates for the preparation of uv and vis wavelength fluorescent probes. Monatshefte Chem. **129**, 777–786 (1998)
23. J. Liu, V. Kepe, A. Zabjek, A. Petric, C.P. Henry, N. Satyamurthy, J.R. Barrio, H.C. Padgett, High-yield, automated radiosynthesis of 2-(1-{6-[(2-[18*F*] fluoroethyl)(methyl)amino]-2-naphthyl}ethylidene)malononitrile ([18F]FDDNP) ready for animal or human administration. Mol. Imaging Biol. **9**, 6–16 (2007)
24. W. West, A.L. Geddes, The effects of solvents and of solid substrates on the visible molecular absorption spectrum of cyanine dyes. J. Phys. Chem. **68**, 837 (1964)
25. W. Klunk, R. Jaccb, R. Mason, Quantifying amyloid β-peptide (Aβ) aggregation using the Congo Red-Aβ (CR–Aβ) spectrophotometric assay. Anal. Biochem. **266**, 66–76 (1999)
26. R.Q. Li, *Specrtral analysis of organic structures*, 1st edn. (Tianjin University press, Tianjin, 2002)
27. R. Christian, Solvatochromic dyes as solvent polarity indicators. Chem. Rev. **94**, 2319–2358 (1994)

28. L. Huang, D.Q. Yu, *The application of UV spectra in the organic chemistry*, 2nd edn. (Science Press, Beijing, 1988)
29. W. Gregorio, J.F. Fay, Synthesis and spectral properties of a hydrophobic fluorescent probe: 6-propionyl-2-(dimethylamino)naphthalene. Biochemistry **18**, 3075–3078 (1979)
30. E.S. Voropai, M.P. Samtsov, K.N. Kaplevskii, A.A. Maskevich, V.I. Stepuro, O.I. Povarova, I.M. Kuznetsova, K.K. Turoverov, A.L. Fink, V.N. Uverskii, Spectral properties of thioflavin T and its complexes with amyloid fibrils. J. Appl. Spectrosc. **70**, 868–874 (2003)
31. C.H. Heo, K.H. Kim, H.J. Kim, S.H. Baik, H. Song, Y.S. Kim, J. Lee, I. Mook-jung, H.M. Kim, A two-photon fluorescent probe for amyloid-b plaques in living mice. Chem. Commun. **49**, 1303–1305 (2013)